

Effects of a Postweld Heat Treatment on a Submerged Arc Welded ASTM A537 Pressure Vessel Steel

Vera Lúcia Othéro de Brito, Herman Jacobus Cornelis Voorwald, Nasareno das Neves, and Ivani de S. Bott

(Submitted 30 January 2001)

Postweld heat treatment (PWHT) is frequently applied to steel pressure vessels, following the requirements of the ASME code (section VIII), which establishes the parameters of the PWHT based on the thickness and chemical composition of the welded section. This work shows the results of an analysis undertaken on a sample of ASTM A537 C1 steel subjected to qualifying welding procedure tests including PWHT (650 °C/5 h). The results obtained showed that this PWHT practice promoted a reduction in the mechanical properties of the base metal and the heat-affected zone (HAZ).

Keywords microalloyed steels, postweld heat treatment, pressure vessels, submerged arc welding

1. Introduction

The aim of this work is to evaluate the effect of a postweld heat treatment (PWHT) on the microstructure and mechanical properties of the base metal, heat-affected zone (HAZ),[1] and weld metal of an submerged arc welded pressure vessel steel. The plate studied was supplied by Confab Industrial S.A-Equipment Division, and the welding and PWHT parameters were selected according to a qualifying welding procedure for a pressure vessel assembled and welded by this manufacturer. Problems have arisen from this PWHT practice, in respect to the toughness of the HAZ and the base metal. In some cases, the energy absorbed by the Charpy specimens of these regions was too low and plates were rejected. It has been observed that the response to PWHT may vary in the different regions of the weld. The PWHT may elevate the toughness of the weld metal, while at the same time reducing this mechanical property of the base metal. This dissimilarity may form a "weak link" in the welded zone. The aim of this work is to analyze this problem in more detail.

The parameters for PWHT in pressure vessels usually follow the ASME code, which assesses holding time and temperature according to the thickness and chemical composition of the steel. Some factors must be taken into account when selecting the parameters for qualifying the welding procedure.

- The pressure vessel to undergo PWHT may contain dissimilar thicknesses and the parameters for the thicker section shall prevail.
- The pressure vessel may undergo future repairs, which will cause a cumulative PWHT effect. Thus, the parameters of the PWHT for the qualifying procedure must predict and simulate this effect.

With respect to the microstructure, the main factors influencing the mechanical properties of a C-Mn welded joint are the following:

- the morphology of the ferrite in the HAZ and weld metal;
- the presence of microphases as the martensite-austenite (MA) constituent and ferrite-carbide aggregate, the former being more detrimental to mechanical properties than the latter;[2,4] and
- the occurrence of precipitation hardening, due to the effects either of a PWHT or the reheating[3] during a subsequent pass in multipass welding.

The effects of a PWHT on the microstructure of a ferritic weld include the tempering of the microstructure, precipitation hardening, and, depending on the temperature of PWHT, the decomposition of MA constituents.[5] The overall result on the mechanical properties will be defined by the magnitude of each possible effect of the PWHT.

2. Experimental Procedure

2.1 Material

The material studied was a plate of ASTM A537 C1 steel, welded by the submerged arc welded multipass process. The F7P8-EH12K wire combination was selected according to the AWS (American Welding Society) classification. The chemical compositions of the base metal and weld metal are shown on Table 1. The welding parameters specified in the SAW process were current = 600 A, voltage = 28/29 V, and travel speed = 45 cm/min. These parameters resulted in a heat input of 22.8 kJ/cm. The groove had a "K" geometry the dimensions of which are shown on Fig. 1. After welding, the plate was cut into two pieces and one of the parts was subjected to PWHT at 650 °C during 5 h.

Vera Lúcia Othéro de Brito and **Herman Jacobus Cornelis Voorwald,** Faculdade de Engenharia Química de Lorena, Departamento de Engenharia de Materiais (DEMAR/FAENQUIL), Pólo Urbo-Industrial, Gleba AI-6, Lorena-SP-Brazil - 12600-000; **Nasareno das Neves,** Faculdade de Tecnologia de São Paulo-Fatec/Unesp e Confab Ind S/A, Departamento de Qualidade, Soldagem e Materiais; and **Ivani de S. Bott,** Pontifícia Universidade Católica do Rio de Janeiro, Departamento de Ciência dos Materiais e Metalurgia (PUC-Rio/DCMM). Contact e-mail: verabrito@usa.net.

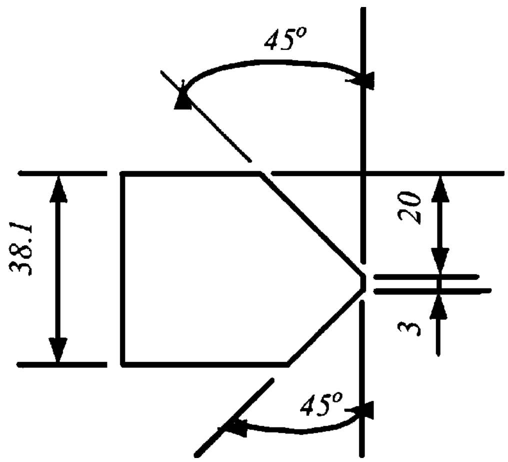

Fig. 1 Groove dimensions (mm)

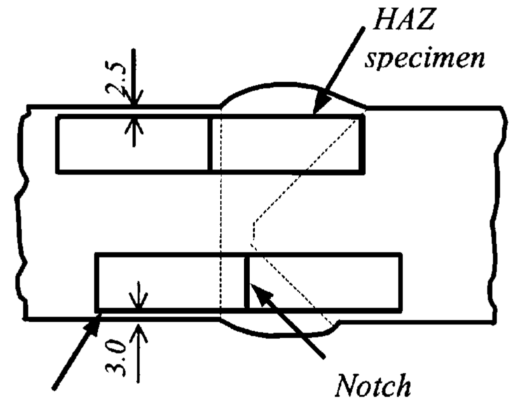

Fig. 2 Location of Charpy specimens (mm)

Fig. 3 Locations of microhardness indentations

Table 1 Chemical analysis of the base metal and the weld metal (wt.%)

Location	C	Mn	Si	Al	S	P	Ti	V	Cr	Mo	Ni	Cu	Nb	CE(a)
Base metal	0.16	1.317	0.188	0.015	0.005	0.014	0.008	0.003	0.020	*traces*	0.144	0.008	0.019	0.46
Weld metal	0.08	1.40	0.009	0.018	0.004	0.009	0.003	0.004	0.021	0.004	0.064	0.058	0.007	…

(a) $CE(IIW) = C + \frac{Mn}{6} + \frac{Cr + Mo + V}{5} + \frac{Ni + Cu}{15}$

2.2 Mechanical Tests

Tensile tests were carried out on the base metal, testing one transverse ASTM subsize specimen (round sections of 8.75 mm diameter) from each plate. The location of extraction of the specimens followed the recommendations of ASTM A 20/A 20M.

The toughness of the weld metal, HAZ, and base metal was evaluated by means of a Charpy impact test, using full size specimens that were machined according to ASTM A370 standard. The notches of the weld metal specimens were placed in a region that contained approximately 70% of columnar microstructure and 30% of reheated microstructure. After each test, the percentage of shear fracture area was measured on the fracture surface of the specimens. The positions on plate from which the Charpy specimens were machined are shown in Fig. 2. The specimens for the testing of the base metal were also transverse specimens, machined from 0.5 mm below the plate surface.

The impact tests were carried out at CONFAB, following the API (American Petroleum Institute) standard (the maximum value of absorbed energy taken, as a result of a test, was 80% (240 J) of the test machine capacity). Three specimens were tested at each one of the seven test temperatures.

Vickers hardness measurements (five indentations) were made on the base metal and weld metal, using a 10 kg load. Vickers microhardness testing with a 40 g load was undertaken on the coarse-grained HAZ (CGHAZ) of the top bead (20 indentations) and on the root pass of the back gouged side (10 indentations). Figure 3 shows the locations where the microhardness indentations were made.

2.3 Light and Scanning Electron Microscopy Examination

Microstructural examination was carried out by optical microscopy and micrographs were taken of the base metal, HAZ, and weld metal. The etchant used was nital 2%. Point

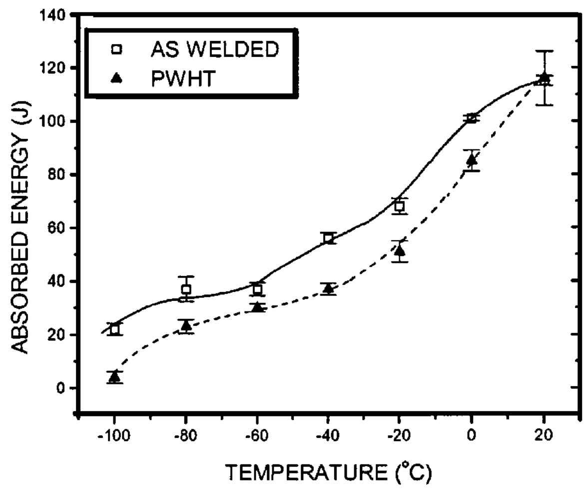

Fig. 4 Absorbed energy curves for the base metal

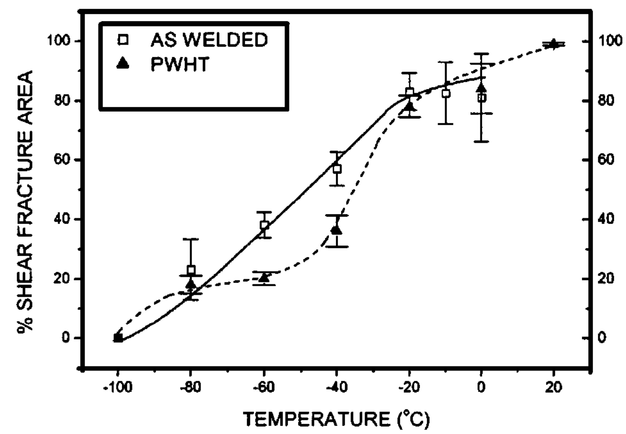

Fig. 5 Percentage of shear fracture area curves for the base metal

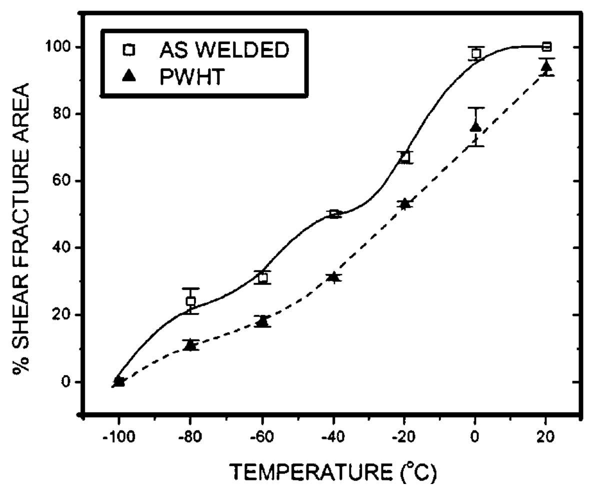

Fig. 6 Absorbed energy curves for the HAZ

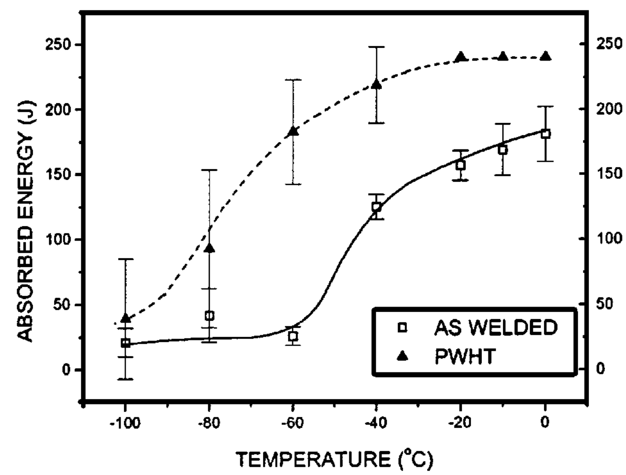

Fig. 7 Percentage of shear fracture area curves for the HAZ

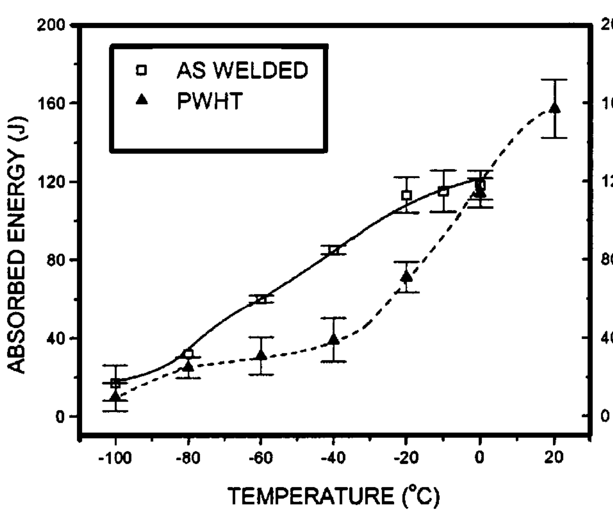

Fig. 8 Absorbed energy curves for the weld metal

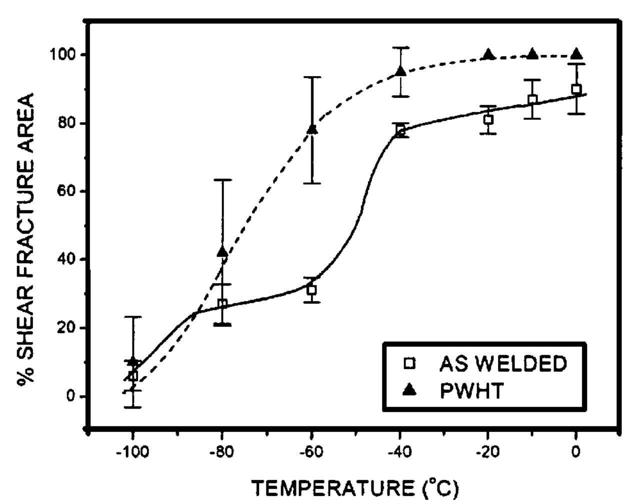

Fig. 9 Percentage of shear fracture area curves for the weld metal

Table 2 Results from tension tests on base metal

Condition	YS (MPa)	TS (MPa)	Elongation (%)
As welded	395	558	33.1
After PWHT	351	502	33.4
Required[8]	345 (minimum)	485–620	22 (in 2 in.)

Table 3 Estimated FATT 50% (°C)

Location	As welded	After PWHT
Base metal	−48	−33
HAZ	−48	−40
Weld metal	−50	−75

counting was carried out on optical micrographs in order to evaluate the morphology of the ferrite in the columnar region of the weld metal. The fields selected for counting were chosen from the top bead. The procedure for point counting followed the IIW recommendations.[7]

Scanning electron microscopy (SEM) was used to observe fracture surface morphologies and to obtain images for quantitative analysis of the MA constituent present in the CGHAZ and the weld metal of the top bead. The fracture images were taken from the center of specimens tested at −60 °C, this temperature being chosen as being within the range of transition temperatures. Ikawa's etching technique[6] was used to enhance the contrast of the MA constituent. The area fraction of the MA constituent was estimated by point counting, applying a 400-point grid over each image at a magnification of 5000×. The point counting was carried out on around 50 images per region (HAZ and weld metal).

3. Results

3.1 Mechanical Tests

The results of tensile tests on the base metal are shown in Table 2. The PWHT reduced both yield (YS) and tensile strength (TS), but the standard requirements were still fulfilled, although near the lower limits. In addition, PWHT reduced the mean value of hardness of the base metal from 167 to 157 HV (6% drop) and of weld metal from 205 to 156 HV (24% drop).

Figures 4 to 9 show the absorbed energy and percentage of shear fracture versus temperature curves. Based on the percentage of shear fracture area curves, fracture appearance transition temperatures (FATT 50%) were estimated and the results are shown in Table 3.

As can be seen, the PWHT reduced the toughness of the base metal and the HAZ. In the base metal, the average absorbed energy was lower for all temperatures after PWHT. The minimum reduction was 16% at 0 °C and the maximum reduction was 82% at −100 °C. The base metal showed a decrease in the lower shelf energy after PWHT. By contrast, PWHT elevated the weld metal absorbed impact energy. The minimum increase was 33% at 0 °C and the maximum increase was 700% at −60 °C. In the case of the HAZ, the average absorbed energy results tended to be lower for temperatures lower than approximately 0 °C and the maximum drop in toughness was 54% at −40 °C. The fracture surfaces of the Charpy specimens observed are shown in Fig. 10 to 15. The base metal, HAZ, and weld metal showed fractures with a quasi-cleavage aspect, the HAZ fracture after PWHT exhibiting a higher number of facets.

The PWHT enlarged the scatter of the impact test results from the weld metal in the transition zone and extended the upper shelf to lower temperatures. The PWHT also enlarged the scatter of the results for the HAZ at temperatures between −40 °C and −80 °C.

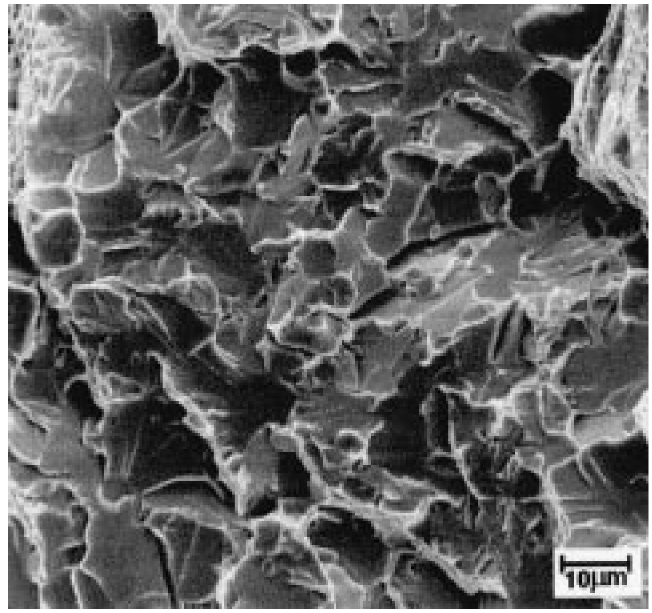

Fig. 10 SEM micrograph of the base metal fracture (as welded)

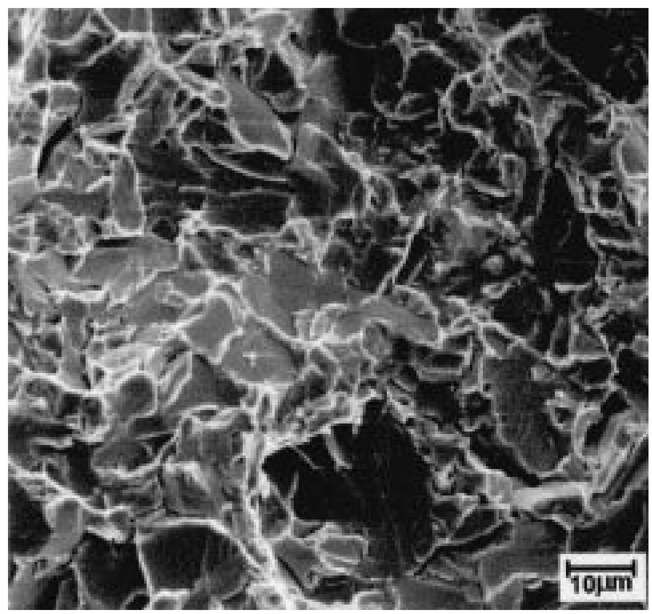

Fig. 11 SEM micrograph of the base metal fracture (PWHT)

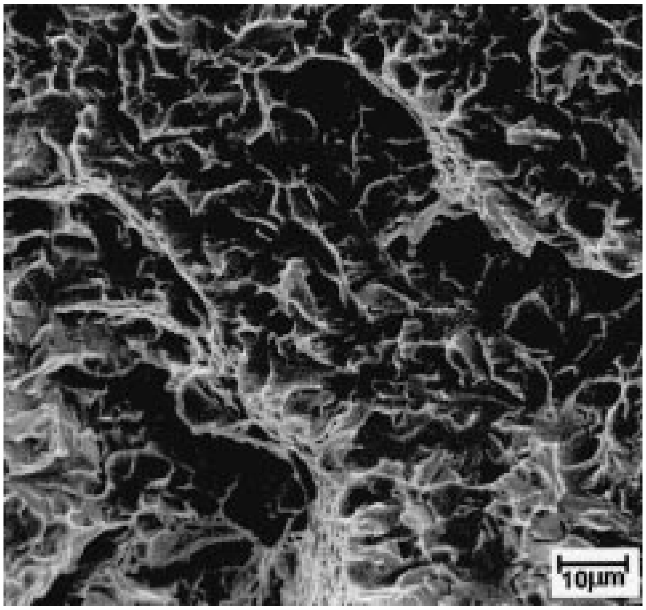

Fig. 12 SEM of the HAZ fracture (as welded)

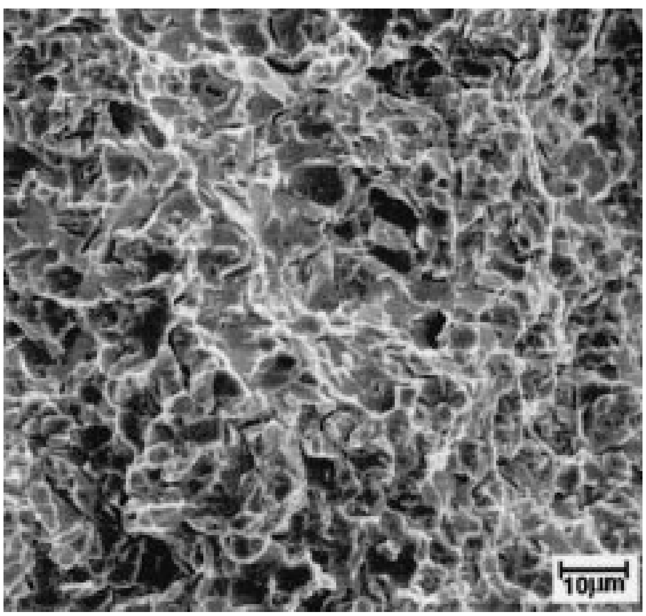

Fig. 13 SEM of the HAZ fracture (PWHT)

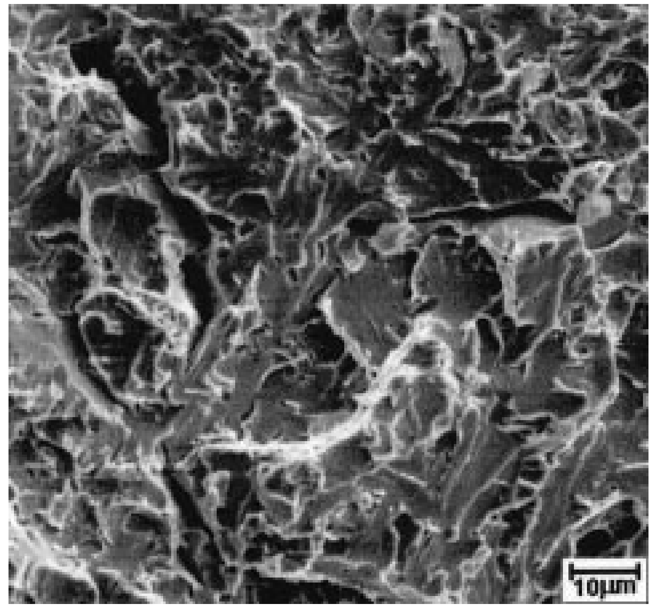

Fig. 14 SEM of the weld metal fracture (as welded)

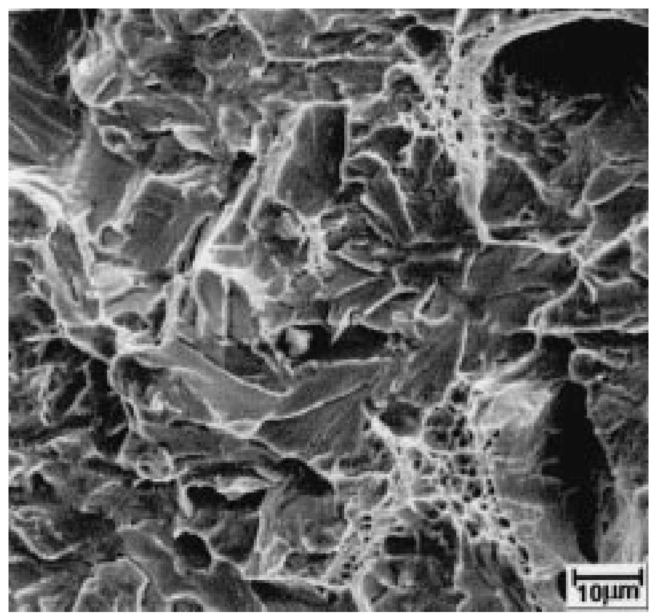

Fig. 15 SEM of the weld metal fracture (PWHT)

The results for microhardness tests are shown in Table 4. One can notice that the HAZ on the second pass of the back gouged side of the sample tested is harder and that the PWHT softened the HAZ in both regions.

3.2 Microstructure

The microstructures observed by optical microscopy of the base metal, CGHAZ, and weld metal are shown in Fig. 18 to 24. Comparing Fig. 16 to Fig. 17, it is possible to notice that the carbides in the pearlite seem to have spheroidized in the base metal after PWHT. At higher magnification (Fig. 18), some intergranular precipitation is apparent.

The microstructure of the CGHAZ of the top bead (Fig. 19) is predominantly constituted of FS (A). After PWHT (Fig. 20), the microstructure is still the same, but the outlines of the FS (A) laths are less visible.

The microstructure of the weld metal is shown in Fig. 21 and 22. The results of the quantitative analysis by optical microscopy are 70.1% acicular ferrite, 5.3% ferrite with second phase (FS), and 25.6% primary ferrite. Figure 22 shows the presence of intragranular precipitates in the weld metal after PWHT.

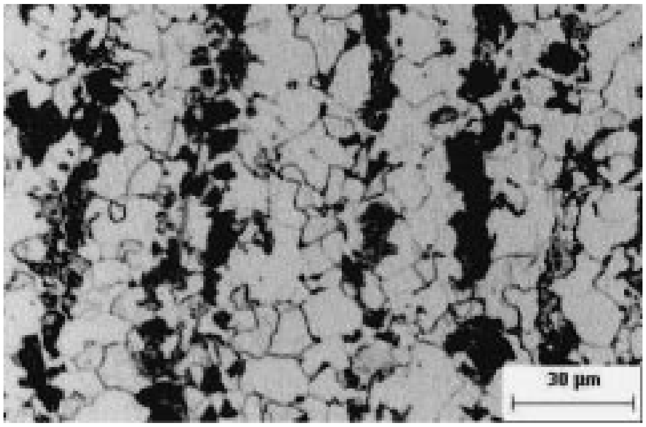

Fig. 16 Optical micrograph (OM) of the base metal microstructure before PWHT

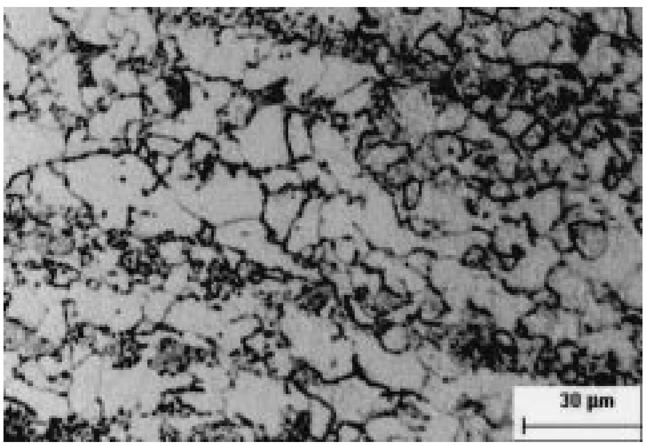

Fig. 17 OM of the base metal microstructure after PWHT

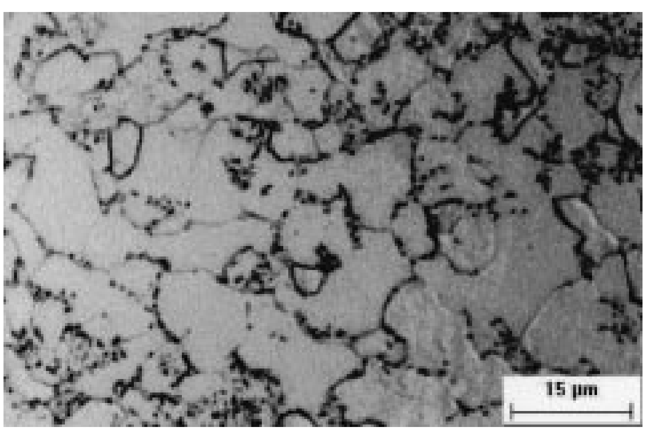

Fig. 18 OM of the base metal microstructure after PWHT

The results for MA constituent counting are shown in Table 5 and SEM micrographs are shown in Fig. 25 to 28. The MA constituents present in the weld metal and in the HAZ are of small size (usually smaller than 1 μm) and sparsely distributed.

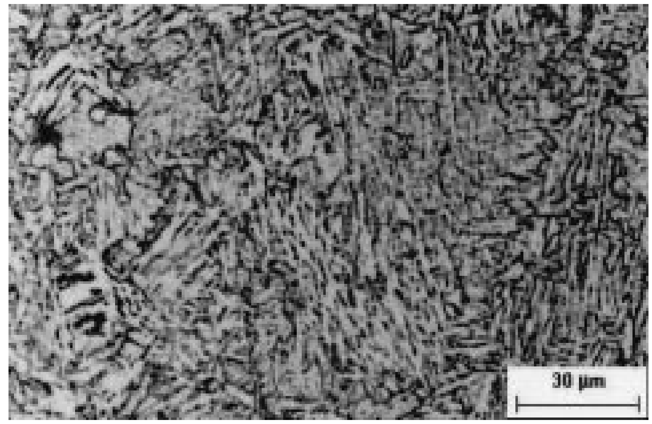

Fig. 19 OM of the CGHAZ microstructure (as welded)

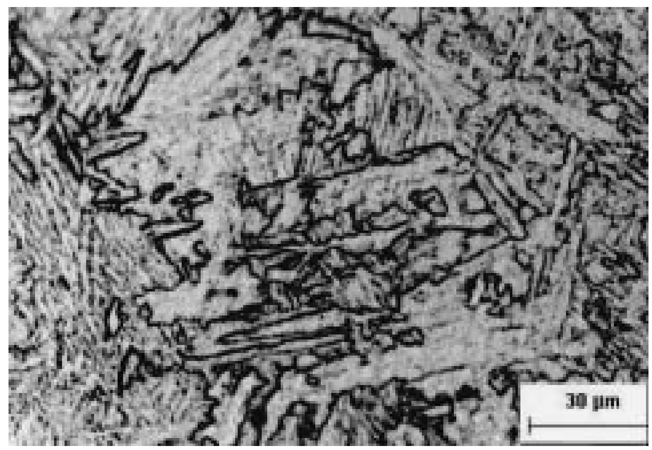

Fig. 20 OM of the CGHAZ microstructure after PWHT

Table 4 Microhardness results

	Average		Standard deviation	
Location	**AW (a)**	**PWHT**	**AW (a)**	**PWHT**
Top bead	250	228	13.2	14.7
Root pass of the back gouged side	309	273	21.2	20.3

(a) AW = as welded

4. Discussion

Based on the work of Sparkes,[12] a drop in the tensile properties of the base metal was expected. This author found that the strength of a C-Mn-Nb and a C-Mn-Nb-V pressure vessel steel tended to deteriorate when the temperature of the PWHT exceeded 600 °C. However, in spite of the drop in strength, the base metal studied here still fulfilled the ASME requirements after PWHT.

It is known from the literature[9–12] that the effect of a PWHT

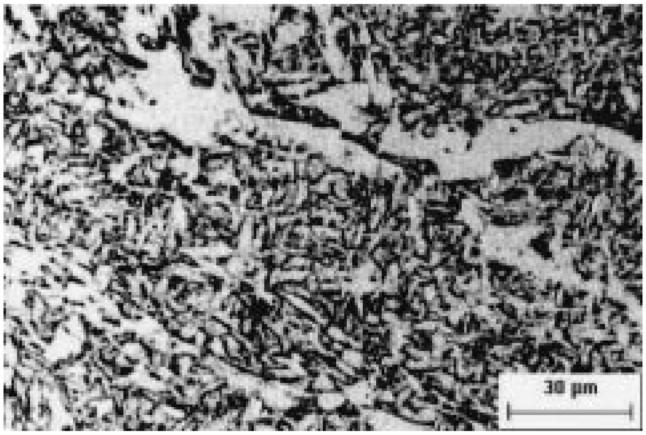

Fig. 21 OM of the weld metal microstructure (as welded)

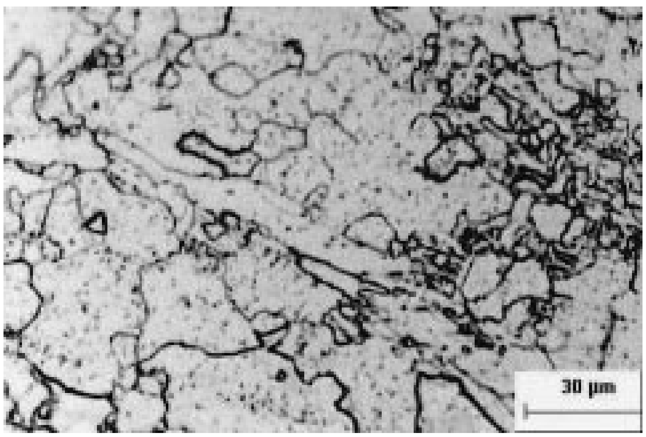

Fig. 22 OM of the weld metal microstructure after PWHT

Fig. 23 OM CGHAZ microstructure of the root pass of the back gouged side (as welded)

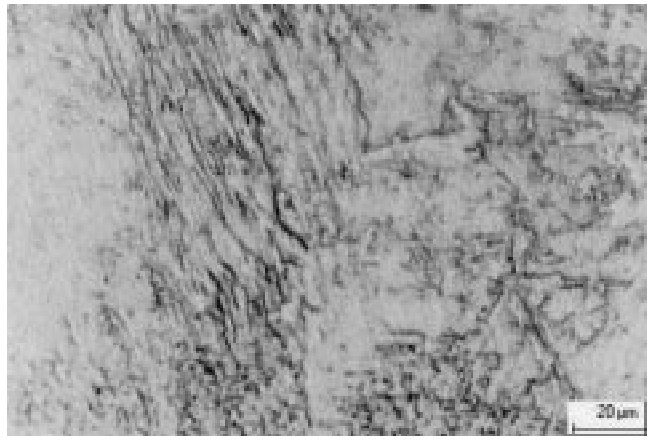

Fig. 24 OM CGHAZ microstructure of the root pass of the back gouged side (PWHT)

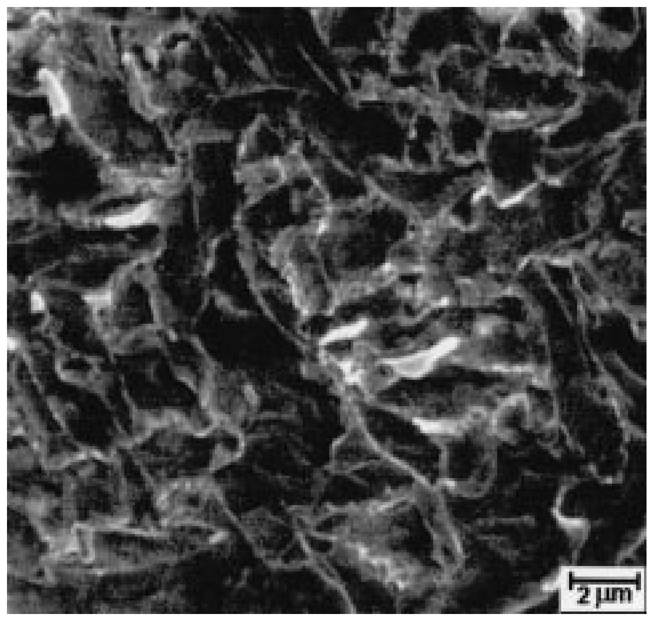

Fig. 25 SEM micrograph of the weld metal (as welded)

Table 5 Area fraction (%) of MA constituent

	HAZ	Weld metal
As welded	0.5	1.3
After PWHT	0.4	<0.1

on the hardness of a weld can vary, according to many factors such as the chemical composition, the weld heat input, and the parameters of PWHT. In general, the weld metal hardness is expected to increase when the Nb content is higher than 0.015%,[9] although this is not the case for the material studied here. In the case of the HAZ, the effect of the PWHT will be more noticeable when martensitic areas are present. The hardness of these areas will decrease due to the tempering effect. Here, the higher hardness of the HAZ of the root pass of the back gouged side was probably due to the cooling rate having been higher for this first pass. This difference in cooling rate existed because the preheat temperature (100 °C) was lower than the interpass temperature (250 °C). The microhardness

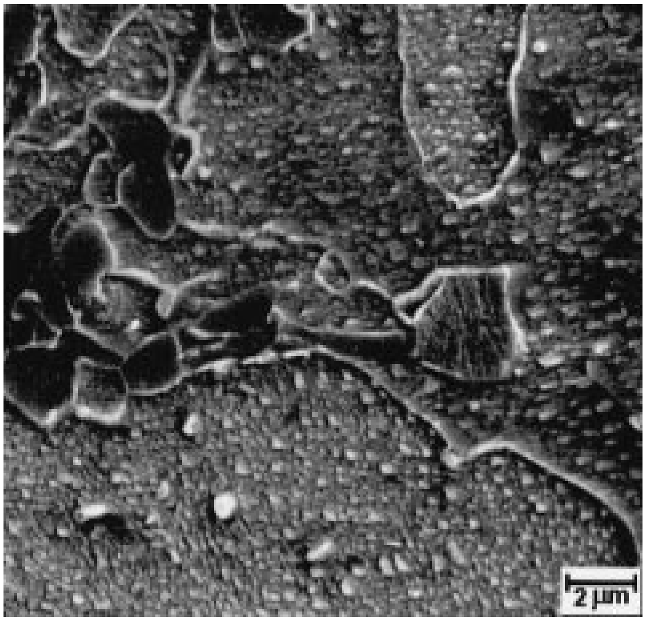

Fig. 26 SEM micrograph of the weld metal after PWHT

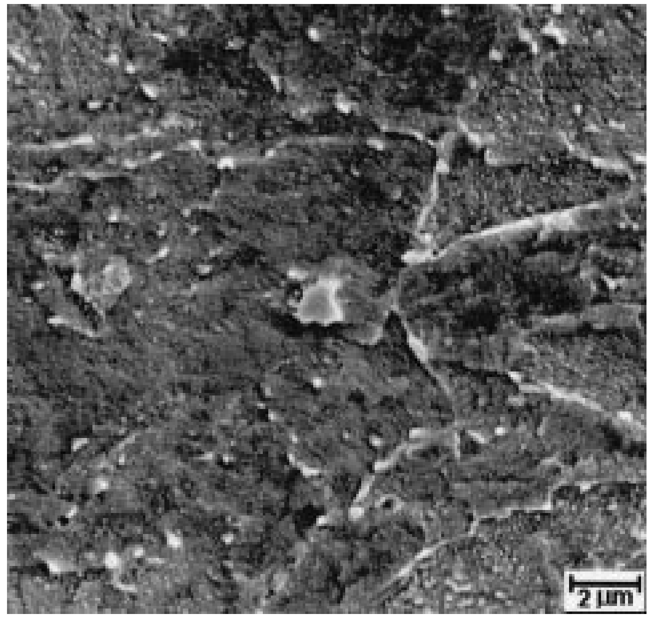

Fig. 28 SEM micrograph of the HAZ after PWHT

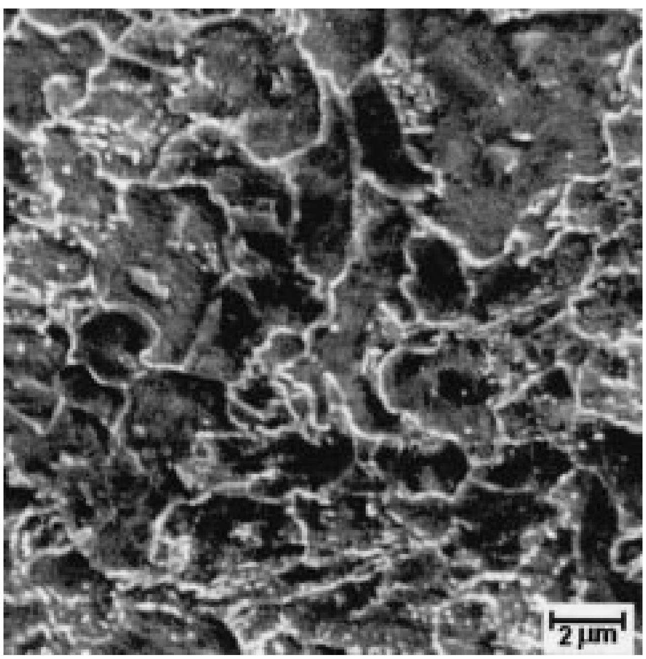

Fig. 27 SEM micrograph of the HAZ (as welded)

values and the appearance of the microstructure indicate that there is some martensite in this region.

Several authors[9–15] have reported the detrimental effects on the toughness of steel caused by precipitation hardening after the PWHT. However, some other phenomena resulting from the PWHT (such as the stress relief effect) can counterbalance this disadvantage of the PWHT. The results presented here indicate that the uniform intragranular precipitation shown in the microstructure of the weld metal did not cause hardening or the impairment of toughness. However, the toughness of the base metal and of the HAZ was affected, probably by intergranular precipitation.

Another important factor affecting the toughness of the welded joint is the presence of MA constituents, mainly in the weld metal and the HAZ, which may act as local brittle zones. However, the amount of MA constituents present in the steel studied was practically negligible. Moreover, the amount of acicular ferrite in the weld metal is in the optimum range cited in the literature[16] (50 to 70%).

Farrar and Ferrante[15] have plotted a diagram from which one can expect that a weld metal containing less than 0.02% Nb may suffer a decrease in FATT after PWHT. This may explain the drop in FATT (50%) of the weld metal studied here, which contains only 0.007% Nb. This value of 0.02% Nb reported by Farrar and Ferrante agrees with the paper of Entrekin,[14] which, in addition, states that toughness reduction will occur after PWHT when finely dispersed coherent precipitates are formed. Entrekin also concluded that toughness reduction will not be noticeable when the precipitates grow, lose coherence, and when there is coalescence. The considerable difference in toughness between the heat-treated weld metal and the other heat-treated regions may have a relationship with chemical composition. The amounts of C and Nb in the base metal are higher, which allows a more intense precipitation of Nb carbides.

For the material and welding conditions studied here, the ASME code sec. VIII div. 1 requires 30 J as the minimum average result of three Charpy impact tests in full size specimens. The minimum individual result established is 20 J. Table 6 shows the 30 J temperature estimated from the absorbed energy curves.

Of the test temperatures used in this work, −60 °C was the lower temperature, in the as-welded condition, that allowed the welded joint to be in accordance with the ASME code sec. VIII div. 1 and −40 °C after the PWHT.

Table 6 30 J temperatures (°C), estimated from the absorbed energy × temperature curves

	As welded	PWHT
Base metal	−91	− 57
HAZ	−77	− 48
Weld metal	−62	<−100

5. Conclusions

The plate studied, welded with a heat input of 22.8 kJ/cm in the SAW process, presented the following characteristics regarding mechanical properties.

- Reduced tensile properties for the base metal. However, both yield strength and tensile strength were slightly above the lower limits established by ASTM. This reduction was expected, based on the literature.
- Higher toughness for the weld metal and a reduction of this property for the HAZ and base metal. This trend was probably observed due to a difference in the characteristics (intensity and location) of the precipitation in these regions.

The parameters employed for PWHT (650 °C/5 h) rendered the material unsuitable for applications at temperatures lower than −40 °C.

Acknowledgments

The authors are grateful for the support and collaboration given by CAPES, CNPQ, CONFAB IND S/A, UNESP-FEG, and Ana Paula M.B. Hashimoto.

References

1. V.L.O. Brito: "Toughness Study of the Submerged Arc Weld HAZ in ASTM A537 C1 Steel and API 5L X70 Linepipes," Master's Thesis, FEG-UNESP, Guaratingueta-SP-Brazil, 1999 (in Portuguese).
2. A.M. Barnes: "The Effect of Intercritical Thermal Cycles on HAZ Microstructure and Toughness in C-Mn-Al-Nb Steel." TWI Research Report No. 402, TWI, Cambridge, 1989.
3. D.J. Sparkes: "Effect of Intercritical Reheating during Welding on the HAZ Microstructure and Toughness in a C-Mn-Nb-Al Steel," TWI Research Report No. 352, TWI, Cambridge, 1987.
4. A.M. Barnes: "Microstructural Development in the Intercritically Reheated Grain Coarsened Heat-Affected Zone of C-Mn Steels," Technology Briefing (TWI), TWI, Cambridge, Dec. 1993.
5. F. Matsuda, K. Ikeuchi, Y. Fukada, Y. Horii, H. Okada, T. Shiwaku, C. Shiga, and S. Suzuki: *Trans. JWRI,* 1995, vol. 24 (1), pp. 1-24.
6. H. Ikawa, H. Oshige, and T. Tanoue: "Effect of Martensite-Austenite Constituent on HAZ Toughness of a High Strength Steel," IIW Document No. IX-1156-80, IIW, France, 1980.
7. *Guide to the Light Microscope Examination of Ferritic Steel Weld Metals,* IIW Document No. IX-1533-88, IIW, France, June 1988, p. 22.
8. *Standard Specification for Pressure Vessel Plates, Heat-Treated, Carbon-Manganese-Silicon Steel,* ASTM A 537/A 537M, ASTM, Philadelphia, PA, 1995.
9. C. Shiga, A. Gotoh, T. Kojima, Y. Horii, Y. Fukada, K. Ikeuti, and F. Matuda: *Welding World,* 1996, vol. 37 (4), pp. 17-29.
10. P.L. Threadgill and R.H Leggatt: "Effects of Postweld Heat Treatment on Mechanical Properties and Residual Stress Levels of Submerged-Arc Welds in a C-Mn-Nb-Al Steel," TWI Research Report No. 253, TWI, Cambridge, 1984.
11. C. Smith, P.G.H. Pistorius, and J. Wannenburg: *Int. J. Pres. Ves. Piping,* 1997, vol. 70, pp. 183-95.
12. D.J. Sparkes: "Effect of a Postweld Heat Treatment on HAZ Microstructure and Toughness of Microalloyed C-Mn Submerged-Arc Welds," TWI Research Report No. 323, TWI, Cambridge, 1986.
13. J.G. Garland and P.R. Kirkwood: *Met. Constr.,* 1975, May, pp. 275-83.
14. C.H. Entrekin: *Welding J.,* 1983, Aug., pp. 197-203.
15. R.A. Farrar and M. Ferrante: *J. Mater. Sci.,* 1982, No. 17, pp. 2405-12.
16. J.T.F. Jorge, L.F.G. Souza, and J.M.A. Rebello: *XIX Encontro Nacional de Tecnologia da Soldagem,* Águas de São Pedro-SP-Brazil, 1993 (in Portuguese).